LA-UR-25-23422
Accepted Manuscript

Microscopic modeling of direct pre-equilibrium emission: Impact on exclusive and inclusive (n,xn) and fission channels

Dupuis, Marc
Capote, Roberto
Kawano, Toshihiko
Kerveno, Maëlle
Desssagne, Philippe
Henning, Greg
Hilaire, Stéphane

Provided by the author(s) and the Los Alamos National Laboratory (2025-07-01).

To be published in: EPJ Web of Conferences

DOI to publisher's version: 10.1051/epjconf/202429204003

Permalink to record:
https://permalink.lanl.gov/object/view?what=info:lanl-repo/lareport/LA-UR-25-23422

Los Alamos National Laboratory, an affirmative action/equal opportunity employer, is operated by Triad National Security, LLC for the National Nuclear Security Administration of U.S. Department of Energy under contract 89233218CNA000001. By approving this article, the publisher recognizes that the U.S. Government retains nonexclusive, royalty-free license to publish or reproduce the published form of this contribution, or to allow others to do so, for U.S. Government purposes. Los Alamos National Laboratory requests that the publisher identify this article as work performed under the auspices of the U.S. Department of Energy. Los Alamos National Laboratory strongly supports academic freedom and a researcher's right to publish; as an institution, however, the Laboratory does not endorse the viewpoint of a publication or guarantee its technical correctness.

Microscopic modeling of direct pre-equilibrium emission: Impact on exclusive and inclusive (n,*x*n) and fission channels

Marc Dupuis[1,2,*], *Roberto* Capote[5], *Toshihiko* Kawano[3], *Maëlle* Kerveno[4], *Philippe* Dessagne[4], *Grégoire* Henning[4], and *Stéphane* Hilaire[1,2]

[1]CEA, DAM, DIF, F-91297 Arpajon, France
[2]Université Paris-Saclay, CEA, Laboratoire Matière sous Conditions Extrêmes, 91680 Bruyères-Le-Châtel, France
[3]Los Alamos National Laboratory, Los Alamos, New Mexico 87545, USA
[4]Université de Strasbourg, CNRS, IPHC/DRS UMR 7178, 23 Rue du Loess, F-67037 Strasbourg, France
[5]Nuclear Data Section, International Atomic Energy Agency, Wagramer Strasse, A-1400 Vienna, Austria

Abstract. We report on a microscopic modeling of the first order of multistep direct emission based on one phonon excitations, given by the QRPA model, and an effective in-medium nucleon nucleon interaction, described within the JLM folding model. The results of our coupled channels framework for deformed target are illustrated in the case of low energy discrete state excitations in ^{152}Sm. Pre-equilibrium predictions and their impact on inclusive and exclusive (n,*x*n) cross sections and fission cross sections are discussed for actinides. We discuss the importance of i) collective excitations to describe the neutron emission spectra and of ii) spin distribution of the residual nucleus formed after the neutron pre-equilibrium emission, that is a key ingredient to model the residual nucleus decay.

1 Introduction

The understanding of medium energy nuclear reaction relies on a precise description of direct, pre-equilibrium and compound nucleus (CN) decay mechanisms. Modeling still nowadays involves a great deal of phenomenology and drastic simplifications of the underlying many-body theories. A progress is to reduce the part of phenomenology in the modeling relying on a microscopic description of reaction mechanisms based on effective NN interactions. The present work focuses on the pre-equilibrium emission mechanism modeling at energies below 20 MeV. We describe the first step of multistep direct (MSD) process as a direct excitation of one phonon from the Quasi-Particle Random Phase Approximation (QRPA) approach. Interactions between the nucleon projectile and each target nucleon are accounted for within the Jeukenne Lejeune Mahaux (JLM) folding model using the Bauge *et al.* parameterization

*e-mail: marc.dupuis@cea.fr

© The Authors, published by EDP Sciences. This is an open access article distributed under the terms of the Creative Commons Attribution License 4.0 (https://creativecommons.org/licenses/by/4.0/).

[1] (labeled JLMB). Cross sections are calculated within the distorted wave Born approximation (DWBA) for spherical targets or solving coupled channels (CC) equations for axially deformed targets.

Two aspects of the pre-equilibrium modeling are discussed. The first is the contribution of the pre-equilibrium process to the emission of the first neutron in (n,*x*n) reactions. More precisely, we focus on neutron emission at high energy, which corresponds to the inelastic process with target excitations approximately in the 1-6 MeV energy range. The second point concerns the characteristics of the composite nucleus, which is the excited target that remains after the first neutron emission and which evolves to a compound nucleus. Distributions in excitation energy, spin and parity of this composite system are key information to model further decay mechanisms. At the considered energies, the most important CN decay after a first neutron emission are: second neutron emission [(n,2n) channel], gamma decay modes ([n,n'γ) channels] or second chance fission.

Description of emission at high energy is a long standing issue that has been tackled in the past using various approaches. A common method used by the nuclear data community [2, 3] relies on the combination of the exciton model to describe the pre-equilibrium emission and direct excitation treated by DWBA of collective levels whose properties (excitation energy, spin, parity, deformation lengths) are adjusted to reproduce (n,*x*n) double differential cross sections and time-of-flight neutron distributions from pulsed-sphere experiments [2–4]. Another approach relies on the Tamura Udagawa Lenske pre-equilibrium model QRPA structure model [5]. A last one also relies on the exciton model with an effective particle-hole level density at low energy that emulates the excitation of collective levels [6]. The present JLMB+QRPA approach provides us with a prediction of this high energy emission compatible with existing measurements.

Besides, the present microscopic approach provides us with spin distributions in the residual nucleus while the exciton model does not [7]. The exciton model is usually complemented with an ad-hoc spin distribution that depends on a spin cut-off parameter which values are not well constrained (see for instance refs.[7, 8]). Various examples in (n,n'γ) reaction modeling [7, 9] have illustrated that our microscopic pre-equilibrium model provides realistic spin distributions. We also found that modifications induced by a microscopic pre-equilibrium modeling have a significant impact on the composite nucleus decay. Various cases of exclusive (n,*x*n) as well as fission cross sections for actinides are discussed.

The second section provides the main lines of the pre-equilibrium modeling. Details on the QRPA and CC framework are given in the third section. Inclusive and exclusive (n,*x*n) and fission cross sections are discussed in the fourth section. Conclusions are finally drawn.

2 One step direct pre-equilibrium process

The MSD process is based on the Born development of the transition amplitude associated with a direct inelastic process (see Feshbach, Kerman, Koonin [10] and Bonetti *et al.*[11] for instance). For nucleon scattering at incident energies E_i below 20 MeV, the one step direct process (that corresponds to the first order of the Born expansion) is considered to dominate. The doubly differential cross section for one pre-equilibrium nucleon emitted at an outgoing energy in the range $[E_f - \frac{\Delta}{2}, E_f + \frac{\Delta}{2}]$ in the solid angle $d\Omega_f$ reads

$$\frac{d^2\sigma(\mathbf{k}_i, \mathbf{k}_f)}{d\Omega_f dE_f} = \frac{1}{\Delta} \int_{E_f-\Delta/2}^{E_f+\Delta/2} dE \sum_n \delta(E_i - E - E_n) \frac{d\sigma_n(\mathbf{k}_i, \mathbf{k})}{d\Omega} , \quad (1)$$

with $E_{i/f/} = \frac{\hbar^2 k_{i/f/}}{2\mu}$, and μ the reduced mass of the projectile-target system. The cross section $\frac{d\sigma_n(\mathbf{k}_i, \mathbf{k})}{d\Omega}$ is associated with nucleon inelastic scattering to the discrete excitation $|n\rangle$ of excitation energy E_n.

The determination of the MSD cross section is then replaced by the calculation of direct inelastic cross sections associated with each target excitation. These can be modeled as linear combinations of n particle n hole excitations of an uncorrelated ground state. If the residual interaction is of two-body nature, the one step direct process gives access to one particle-hole components. Here we consider phonon excitations of a correlated ground state defined as the phonon vacuum. We describe those phonon excitations within the QRPA framework which relies on the quasi-boson approximation. Considering the quasi-boson approximation, the two-body residual interaction only connects states with number of phonons that differs of maximum one unity. Consequently, for the one step direct process, final levels are identified to one-phonon excitations. Couplings to configurations that are out of the QRPA framework phase space, are taken into account by associating finite lifetimes with the one-phonon QRPA excitations. These lifetimes result in finite widths Γ_n of the excitations which are accounted for replacing energies E_n in the Dirac distribution δ in (1) with complex energies $E_n + i\Gamma_n$. Dirac distributions are then replaced with Lorentz distributions. Widths Γ_n are determined using an empirical approach based on the experimental knowledge of level widths for various giant resonances [12].

Individual cross sections in the case of spherical targets are determined within the DWBA framework: excitations of discrete levels described as QRPA one phonon excitation in (n,n') and (p,p') reaction within the JLMB framework were previously discussed (see [13] and refs therein). For targets with a large axial elongation, CC needs to be considered. We calculate inelastic scattering to one phonon excitations accounting for CC effects between two rotational bands: the first built on the target ground state and the second built on a one phonon excitation. We discard CC effects between two rotational bands built on one phonon excitation. Indeed, introducing larger coupling schemes would require tailoring new effective interactions, since the JLMB model effective interaction already implicitly accounts for couplings to all intrinsic excitations.

3 JLMB+QRPA coupled channels approach for inelastic scattering to discrete excitations

3.1 Main lines of the theory

The theory that describes elastic and inelastic scattering to a few discrete excitations from a model wave function and an effective two-body interaction, from which a set of CC equations is defined, is for instance detailed by Satchler [14]. Here, we only remind that the Schrodinger equation that needs to be solved reads $(T + H_A + V_{\rm res} - E)\,|\Psi\rangle = 0$, with T the kinetic energy operator for the target-projectile relative motion, H_A the target Hamiltonian and $V_{\rm res}$ a two-body effective interaction between the nucleon projectile and nucleons of the target. Leaving out the projectile intrinsic state for simplicity, the total model wave function $|\Psi\rangle$ corresponds to a finite sum of products of target states $|n\rangle$, with $H_A|n\rangle = E_n|n\rangle$, and functions φ_n that represent the relative motion states between the target and the projectile for each channel, namely $|\Psi\rangle = \sum_{n=0}^{N} \varphi_n|n\rangle$. Projecting the Shrödinger equation on each target state $|n\rangle$ provides a set of coupled equations. The equation for the channel corresponding to the target state $|n\rangle$ is

$$(T - (E_i - E_n) + U_{nn})\,\varphi_n = -\sum_{n' \neq n} U_{nn'}\varphi'_n\,, \tag{2}$$

where E_n is the excitation energy of the target state $|n\rangle$, and coupling (optical and transition) potentials are $U_{nn'} = \langle n|V_{\rm res}|n'\rangle$. Solving coupled equations provide the φ_n solutions from which observables are calculated. In the present work, the ECIS code [15] is used to solve CC equations. Coupling potentials are calculated from the nuclear structure QRPA and the JLMB folding models [1], as detailed below.

3.2 Nuclear structure input from QRPA

QRPA calculations are performed starting from Hartree-Fock Bogoliubov solutions using the Gogny D1S interaction. Equations are solved in a cylindrical harmonic oscillator basis conserving axial symmetry and parity. QRPA solutions thus have the total angular momentum projection K on the quantization axis as well as the parity Π as good quantum numbers. Details of the QRPA theory are given by Ring and Schuck [16], and Peru *et al* [17, 18] for QRPA framework implemented with Gogny D1-type forces. We remind here that in the deformed QRPA framework, natural excited states of the target are represented by phonon excitations of a correlated ground state $|\tilde{0}\rangle$ in the intrinsic frame. The one phonon excitation reads $|\alpha K\Pi\rangle = \Theta^+_{\alpha K\Pi}|\tilde{0}\rangle$.

Quantum states in the laboratory frame are obtained after projection over the total angular momentum

$$|\alpha JM\Pi\rangle = \sqrt{\frac{2J+1}{16\pi^2}}\int d\Omega \mathcal{D}^{J}_{MK}{}^{*}(\Omega)R(\Omega)|\alpha K\Pi\rangle + (-)^{J+K}\mathcal{D}^{J}_{M-K}{}^{*}(\Omega)R(\Omega)|\alpha \bar{K}\Pi\rangle$$

$$\forall J \geq K \quad \text{if} \quad K > 0\,,$$

$$= \sqrt{\frac{2J+1}{8\pi^2}}\int d\Omega \mathcal{D}^{J}_{M0}{}^{*}(\Omega)R(\Omega)|\alpha 0\Pi\rangle \quad \text{for} \quad K = 0\,, \tag{3}$$

$$\forall J \in \{0,2,4,\cdots\} \quad \text{if} \quad K = 0^+ \quad \text{and} \quad \forall J \in \{1,3,5,\cdots\} \quad \text{if} \quad K = 0^-\,,$$

where $\mathcal{D}$ is the Wigner-D matrix and Ω represents Euler angles. The vector $|\alpha \bar{K}\Pi\rangle$ is the time reversed vector $|\alpha K\Pi\rangle$. For nuclei with a strong axial deformation, states defined by Eq. (3) built from one intrinsic excitation $|\alpha K\Pi\rangle$ can be associated with a rotational band. In the rotational model, excitation energies are given by the approximation $E_{\alpha KJ\Pi} = E_{\alpha K\Pi} + \frac{J(J+1)-K^2}{2\mathcal{I}^2}$ where $E_{\alpha K\Pi}$ is the QRPA excitation energy in the intrinsic frame and $\mathcal{I}$ the nucleus moment of inertia which is approximated here by the HFB moment of inertia.
The matter density associated with the ground state in the intrinsic frame reads

$$\rho(\mathbf{r}) = \langle\tilde{0}_I|\sum_{n=1}^{A}\delta(\mathbf{r_n} - \mathbf{r})|\tilde{0}_I\rangle = \sum_L \rho_L(r)Y^L_0(\theta)\ \,, \tag{4}$$

and the matter density variation associated with the transition between the ground state and one excited state in the intrinsic frame reads

$$\rho^{\tilde{0}_I,\alpha K\Pi}(\mathbf{r}) = \langle\alpha K\Pi|\sum_{n=1}^{A}\delta(\mathbf{r}_n - \mathbf{r})|\tilde{0}_I\rangle = \sum_{L\geq K}\rho^{\tilde{0}_I,\alpha K\Pi}_L(r)Y^{L}_{K}{}^{*}(\theta\phi)\,, \tag{5}$$

where functions $Y(\theta\phi)$ are spherical harmonics. These densities are the main structure input of the JLMB folding model.

3.3 Coupling potentials

With the definition Eq. (3) of laboratory states, and rotating the interaction to act in the intrinsic frame, coupling potentials can easily be expressed in term of matrix elements of the residual interaction between states in the intrinsic frame. For instance, couplings between states belonging to two rotational bands (ground state band and excited band) are calculated from

$$\langle \alpha K\Pi | V_{\rm res} | \tilde{0}_I \rangle = \sum_L U_L^{\tilde{0}_I,\alpha K\Pi}(r_1) Y_K^{L*}(\Omega_1') \ , \tag{6}$$

with

$$U_L^{\tilde{0}_I,\alpha K\Pi}(r_1) = \int V_L(r_1, r_2') \rho^{\tilde{0}_I,\alpha K\Pi}(\mathbf{r}_2) Y_K^{L*}(\Omega_2') r_2' \, dr_2' \, d\Omega_2' \ , \tag{7}$$

where $V_L(r_1, r_2')$ is the $L^{\rm th}$ multipole of the expansion of the density dependent and finite range two-body effective interaction of the JLMB model. Here r_1 is the relative motion coordinate in the center of mass. Coordinates with prime are in the intrinsic frame. Note that selection rules apply to L-values for transitions between an initial state i and final state f: $|J_i - J_f| \leq L \leq J_i + J_f$ and $\Pi_i \Pi_f = (-)^L$ (since the JLMB folding model involves one-body local central and spin orbit potentials). Note also that the rotational approximation [19] is used to express the coupling potentials in the center of mass frame that appears in the CC scheme. Coupling potentials between states within the same rotational band are readily obtained replacing transition densities in Eq. (7) by matter densities, Eq. (4). Here we approximate couplings within an excited band by those calculated within the ground state rotational band.

3.4 Application to ^{152}Sm(p,p)'

While we focus here on neutron scattering observables, studying (p,p') observables allows us to assess the validity of our modeling since i) proton inelastic scattering differential cross sections can be and have been measured for both the ground state and excited bands levels while data for neutron are more scarce; ii) since we use the Lane consistent JLMB folding model [1, 13], description of neutron and proton scattering only differs from the Coulomb component of the potential.

We discuss an example of a CC calculation for the 65 MeV proton scattering on ^{152}Sm considering the $K^\Pi = 0^+$ ground state rotational band and the rotational band built on the lowest energy $K^\Pi = 2^+$ QRPA one phonon intrinsic excitation (gamma band). Calculations are performed with levels up to total angular momentum $J = 8$ and maximum transfered orbital angular momentum $L = 8$, in $\hbar$ units. The CC scheme is illustrated in Fig. 1 (right panel). Figure 1 (left panel) illustrates the very good agreement between calculated and measured differential cross sections for the elastic channel, and the inelastic channels corresponding to the 2^+, 4^+ , 6^+, 8^+ levels of the ground state rotational band. This follows the accurate description of nuclear densities and deformation in the HFB/D1S framework. Experimental and calculated inelastic differential cross sections are compared in Fig. 2 for the excitation of the 2_3^+ and 4_3^+ levels that belong to the gamma-band which is built on the lowest energy $K^\Pi = 2^+$ QRPA one-phonon excitation. CC calculations (full black curves) are in agreement with measurements. QRPA/D1S predictions and experimental reduced transition densities $B(E_L \uparrow)$ values are in good agreement for both excitations: $B(E_2 \uparrow) = 0.101 e^2 b^2$ [QRPA] vs $0.1101(57) e^2 b^2$ (exp [20]) and $B(E_4 \uparrow) = 0.00823 e^2 b^4$ [QRPA] vs $0.01112(74) e^2 b^4$ (exp [20]). This gives us confidence in the nuclear structure information used in our model and explains in part the good results of the reaction model for these two levels.

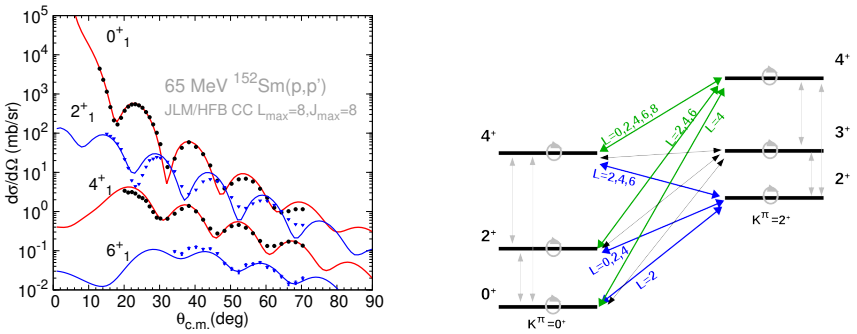

Figure 1. Left panel: 65 MeV proton scattering off ^{152}Sm for the ground state rotational band members (0^+ for elastic, 2^+, 4^+, 6^+ inelastic). JLMB/HFB calculations (curves) are compared to measurements [21] (symbols). Right panel: CC scheme (representation limited to levels up to $J = 4$, calculations include levels up to $J = 8$). Arrows represent coupling potentials $\langle n'|V_{\rm res}|n\rangle$ of Eq. (6). Closed loops are for $n = n'$. The L-multipole potentials components are detailed for transitions between GS rotational band levels and the 2^+ and 4^+ levels belonging to the gamma band.

Accounting for CC effects is also of prime importance. To illustrate this, Fig. 2 also displays calculations performed with the following truncations: a) full calculation, b) calculations that conserve only the $L = 2$ component of the deformed transition density [Eq. (5)], c) same than b) but conserving only the $L = 4$ component in Eq. (5), d) calculations that use the full transition density but a truncated coupling potential [Eq. (6)] conserving only its $L = 2$ component, e) same than d) but conserving only the $L = 4$ transition potential component in Eq. (6), f) same than e) but conserving both the $L = 2$ and 4 transition potential components in Eq. (6). Inelastic scattering to the 2^+_3 level is well described as long as the main components ($L = 2$) of the transition density and the transition potential are conserved (all calculations but cases c) and e) - note that cases a) and f) are indistinguishable). However, for the 4^+_3 level, CC effects are more visible. The full black [case a)] and long dashed orange curves [case f)] almost coincide which shows that calculations should be performed considering at least: both $L = 2$ and 4 transition density components to build the transition potential as well as both the $L = 2$ and 4 coupling potential components to solve the CC equations. Other truncation schemes [cases b,c,d] strongly disagree with measurements. For instance calculations c) and e) cases (only L=4 for transition density or potential) strongly over-predict and b) and d) cases (only L =2 for transition density or potential) strongly under-predict cross sections. This shows that large constructive and destructive interference arises when $L = 2$ to $L = 4$ transition potential components are combined within the CC framework: for instance, direct $L = 4$ transition from the ground state to a 4^+ gamma-band state interfers with second order transitions for which the 2^+ ground band or gamma-band states are intermediate excitations.

4 (n,*x*n) and fission cross sections

The CC approach is applied to all energy accessible QRPA one phonon excitations to determine the doubly differential cross section defined in Eq. (1). Application to ^{239}Pu(n,n') (this case of odd-even nucleus is considered within the weak coupling limit that represents ^{239}Pu levels by one neutron hole on a ^{240}Pu core) is illustrated on Fig. 3 (left panel) which shows the contribution of the direct one-phonon excitation (which represents the one-step direct pre-equilibrium process) to the doubly differential inclusive (n,*x*n) cross section.

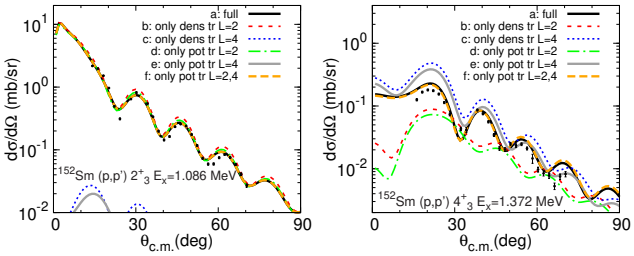

Figure 2. 65 MeV (p,p') off ^{152}Sm to the 2^+_3 (left panel) and the 4^+_3 (right panel) levels that belong to the $K^\Pi = 2^+$ gamma-band. CC calculations (curves) are compared to experimental data [21] (symbols) and to calculations with various truncations on the transition density or potential (see details in text).

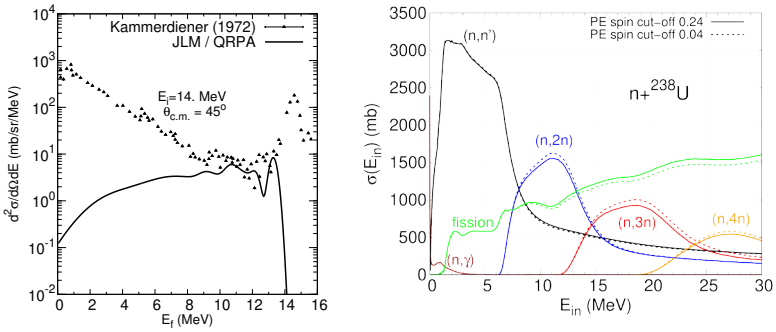

Figure 3. Left panel: calculated direct pre-equilibrium contribution, from the JLMB/QRPA approach (curve), to inclusive (n,*x*n) cross sections for 14 MeV neutron incident on ^{239}Pu at the outgoing angle $\theta_{c.m.} = 45°$. Symbols are experimental data from Kammerdiener [22]. Right panel: fission, (n,n'), (n,2n), (n,3n) and (n,4n) exclusive cross sections for the n+^{238}U reaction. Calculations with the exciton model and a spin cut-off parameter $s = 0.24$ (defined in Eq.(10) of ref. [7]) (full curves) are compared to calculations performed with $s = 0.04$ which approximately corresponds to the JLMB/QRPA model prediction (dashed curves).

Contributions from other reaction mechanisms -namely elastic scattering, direct inelastic scattering to excited levels of the ground state band, compound nucleus emission and neutron evaporated from fission fragments- are not included in the plot. This comparison illustrates that excitations of collective levels, which are predicted by our QRPA calculation and included in our microscopic pre-equilibrium model, allows a good description of neutron emission at outgoing energies $E_f = 8 - 13.5$ MeV (which corresponds to target excitation energies $E_n = 0.5 - 6$ MeV), without relying on ad-hoc adjustment procedures.

The JLMB/QRPA approach also provides spin distributions of the residual nucleus after the pre-equilibrium emission of one neutron. This was previously discussed in [7, 23]. These works showed that the JLMB/QRPA model predicts mean spin values of the residual nucleus much smaller than what was previously assumed. The impact on (n,n'γ) cross sections for gamma emission from high spin ($J > 5\hbar$) levels was proven to be quite large and in agreement with measurements. Here we explore another consequence of the reduction of the mean spin of the residual nucleus. In Dupuis et al. [23], it was shown that the spin cut-off parameter inferred from the JLMB/QRPA microscopic calculation can be used to constrained

the empirical spin distribution which is associated with the exciton model. This allows to test the impact of this aspect on all opened reaction channels. Calculations are performed with the TALYS code [24] and model parameters from Romain *et al.* [25]. Figure 3 (right panel) compares calculations performed with the exciton model and the previously assumed spin distribution to calculations with a spin distribution fitted to reproduce the JLMB/QRPA predictions (see details in ref. [7]). The fission cross section is reduced above 8 MeV while all (n,*x*n) cross sections for $x \geq 2$ are increased. Inelastic is practically unchanged. Reduction of the mean spin of the compound system after the pre-equilibrium emission of one neutron changes the competition between the second fission chance and the emission of a second neutron by evaporation. This follows the facts that low spin favors neutron emission and that fission barriers increases when the spin of the fissioning system increases.

5 Conclusion

A microscopic description of the one-step direct process for neutron scattering on spherical and deformed nuclei is performed based on QRPA nuclear structure model implemented with a Gogny force and an effective in medium NN interaction from the JLM folding model. Scattering off strongly deformed target are considered within the coupled channels framework. Coupled channels calculations are illustrated for the ^{152}Sm(p,p') reaction. For neutron scattering on actinides, implications of the present microscopic modeling on inclusive (n,*x*n) doubly differential cross sections, and exclusive (n,2n), (n,3n) and (n,4n) cross sections as well as (n,f) cross sections are illustrated. The low mean spin value predicted in our model in comparison to prescription used in the past implies an increase of the (n,2n), (n,3) and (n,4n) cross sections and in the same time a diminution of the fission cross section at energies beyond 10 MeV, where pre-equilibrium is strong enough to play a significant role.

References

[1] E. Bauge, J.P. Delaroche, M. Girod, Phys. Rev. C **63**, 024607 (2001)
[2] P. Young, M. Chadwick, R. MacFarlane, P. Talou, T. Kawano, D. Madland, W. Wilson, C. Wilkerson, Nuclear Data Sheets **108**, 2589 (2007)
[3] R. Capote, A. Trkov, M. Sin, M. Pigni, V. Pronyaev, J. Balibrea, D. Bernard, D. Cano-Ott, Y. Danon, A. Daskalakis et al., Nuclear Data Sheets **148**, 254 (2018)
[4] L.F. Hansen, C. Wong, T.T. Komoto, B.A. Pohl, E. Goldberg, R.J. Howerton, W.M. Webster, Nuclear Science and Engineering **72**, 35 (1979)
[5] H. Wienke, R. Capote, M. Herman, M. Sin, Phys. Rev. C **78**, 064611 (2008)
[6] M.R. Mumpower, D. Neudecker, H. Sasaki, T. Kawano, A.E. Lovell, M.W. Herman, I. Stetcu, M. Dupuis, Phys. Rev. C **107**, 034606 (2023)
[7] M. Kerveno, M. Dupuis, A. Bacquias, F. Belloni, D. Bernard, C. Borcea, M. Boromiza, R. Capote, C. De Saint Jean, P. Dessagne et al., Phys. Rev. C **104**, 044605 (2021)
[8] D. Dashdorj, T. Kawano, P.E. Garrett, J.A. Becker, U. Agvaanluvsan, L.A. Bernstein, M.B. Chadwick, M. Devlin, N. Fotiades, G.E. Mitchell et al., Phys. Rev. C **75**, 054612 (2007)
[9] E. Party, Ph.D. thesis (2019), study of reactions (n,*x*n) for fertile/fissile nuclei of the innovative Thorium fuel cycle, `http://www.theses.fr/2019STRAE020`
[10] H. Feshbach, A. Kerman, S. Koonin, Ann. Phys. (N.Y.) **125**, 429 (1980)
[11] R. Bonetti, M. Chadwick, P. Hodgson, B. Carlson, M. Hussein, Physics Reports **202**, 171 (1991)

[12] M. Harakeh, A. van der Woude, *Giant Resonances* (Oxford University Press, New York, 2001)
[13] M. Dupuis, G. Haouat, J.P. Delaroche, E. Bauge, J. Lachkar, Phys. Rev. C **100**, 044607 (2019)
[14] G.R. Satchler, *Direct Nuclear Reactions* (Oxford University Press, New York, 1983)
[15] J. Raynal (1994), code ECIS95, unpublished and CEA Report no CEA-N-2772
[16] P. Ring, P. Schuck, *The Nuclear Many-Body Problem* (Springer-Verlag, Berlin Heidelberg, 1980)
[17] S. Péru, H. Goutte, Phys. Rev. C **77**, 044313 (2008)
[18] S. Péru, G. Gosselin, M. Martini, M. Dupuis, S. Hilaire, J.C. Devaux, Phys. Rev. C **83**, 014314 (2011)
[19] J. Libert, M. Girod, J.P. Delaroche, Phys. Rev. C **60**, 054301 (1999)
[20] T. Ichihara, H. Sakaguchi, M. Nakamura, M. Yosoi, M. Ieiri, Y. Takeuchi, H. Togawa, T. Tsutsumi, S. Kobayashi, Phys. Rev. C **36**, 1754 (1987)
[21] F. Ohtani, H. Sakaguchi, M. Nakamura, T. Noro, H. Sakamoto, H. Ogawa, T. Ichihara, M. Yosoi, S. Kobayashi, Phys. Rev. C **28** (1983)
[22] J.L. Kammerdiener, Ph.D. thesis (1972), neutron spectra emitted by 239Pu, 238U, 235U, Pb, Nb, Ni, Al, and C irradiated by 14 MeV neutrons, `https://www.osti.gov/biblio/4669084`
[23] Dupuis, Marc, Kawano, Toshihiko, Kerveno, Maëlle, Hilaire, Stéphane, EPJ Web of Conf. **284**, 03003 (2023)
[24] Koning, Arjan, Hilaire, Stephane, Goriely, Stephane, Eur. Phys. J. A **59**, 131 (2023)
[25] P. Romain, B. Morillon, H. Duarte, Nuclear Data Sheets **131**, 222 (2016)